Journal of Biomolecular NMR, 4 (1994) 653–672
ESCOM

J-Bio NMR 195

Solution structure by ^{1}H and dynamics by natural abundance ^{13}C NMR of a receptor recognising peptide derived from a C-terminal fragment of neuropeptide Y*

Klas Arvidsson, Jüri Jarvet**, Peter Allard and Anders Ehrenberg***

Department of Biophysics, Arrhenius Laboratories, Stockholm University, S-106 91 Stockholm, Sweden

Received 3 January 1994
Accepted 18 February 1994

Keywords: NPY; α-Helix; ^{13}C NMR relaxation; Correlation time; Flexibility; Monomer

SUMMARY

A peptide consisting of 20 amino acid residues, derived from a C-terminal fragment of neuropeptide Y (NPY) and showing high affinity to NPY receptors, was synthesised. Its sequence is PAADLARYRHYINLITRQRY-NH_2, and the solution structure was calculated from NMR-derived distance and torsion angle restraints, obtained at 15 °C in a solvent mixture of water and 30% (v/v) 1,1,1,3,3,3-hexafluoro-2-propanol, by using DIANA and restrained energy minimisation. The structure was found to consist of a well-defined α-helix in the centre, with a few residues at the termini having less well defined conformations. The spin-lattice and spin-spin relaxation rates of α-carbons have been determined on ^{13}C at natural abundance. From 1D experiments the global rotational correlation time was determined and from 2D experiments the dynamics of each individual residue was obtained. The results demonstrate that the C^{α}-H^{α} vectors in the α-helix essentially follow the global motion. Towards the termini, contributions from local dynamics increase. This tendency is correlated to the increasing uncertainty of the structure towards the peptide ends. An effective molecular volume was calculated from the temperature dependence of the global rotational correlation time. This is well compatible with a monomeric peptide, solvated by water and 1,1,1,3,3,3-hexafluoro-2-propanol. The presence of peptide dimers was ruled out as being inconsistent with the relaxation data.

INTRODUCTION

The solution structures of proteins and peptides determined by NMR are usually well defined in major parts, but they often also show sections which are less well defined. Such regions are

*Supplementary material available from the authors: Two data tables and 10 PDB coordinate files of the calculated NMR structures of P7. One data table contains all detected and integrated NOE intensities; the other connects each proton and pseudoatom to an atom number used in the NOE table. The table contents served as input data files for CALIBA.

**Currently on leave from the Institute of Chemical Physics and Biophysics, Tallinn, Estonia.
***To whom correspondence should be addressed.

proposed to have a high degree of flexibility. When superimposing several structures, calculated from the same set of NMR-derived restraints, such regions often reveal themselves as areas where it is not possible to obtain a good fit between the structures. The question arises whether this spread among the calculated structures signifies an intrinsic flexibility of the peptide, or is merely a consequence of too few structural restraints available in those regions.

Another important question concerns the presence of monomeric or dimeric forms, or even larger aggregates, of the peptide in solution at the concentrations necessary for NMR studies. For example, dimer formation of neuropeptide Y (NPY) has been proposed by Cowley et al. (1992) from analysis of NMR data, collected in H_2O at pH 3.2, 37 °C (Saudek and Pelton, 1990). The formation of NPY dimers has also been inferred from measurements of sedimentation equilibria (Krstenansky and Buck, 1987; Minakata et al., 1989) and CD (Minakata et al., 1989). Conversely, studying NPY by NMR in the strong helix-promoting solvent 2,2,2-trifluoroethanol (100%), Mierke et al. (1992) did not find any evidence for dimer formation. It is thus important to measure both global and local dynamics of a peptide in the same solvent in which its structure is being determined.

During the course of our studies on NPY and NPY-related peptides (Arvidsson et al., unpublished results) it became desirable to answer both types of question mentioned above. Here we present the results of an investigation with this goal. For this study we have chosen a peptide related to NPY. The sequence of this peptide is based on the C-terminal section NPY(13–36)amide, where the four residues Tyr^{21}-Leu^{24} are deleted and Glu^{15} is replaced by alanine. This peptide, P7, has the sequence PAADLARYRHYINLITRQRY-NH_2, and was found to retain a high affinity to NPY receptors from rat hippocampal membranes, with IC_{50} = 4.0 nM as compared with 0.8 nM for NPY itself (Arvidsson et al., unpublished results). From comparisons with other related peptides, we had reason to believe that this peptide should form a quite stable α-helix. We have found this to be true in water/1,1,1,3,3,3-hexafluoro-2-propanol (70/30% v/v) on the basis of CD measurements and the ^1H NMR-determined structure. The global and local dynamics of P7 were derived from ^{13}C spin-spin and spin-lattice relaxation rates, which were determined using ^{13}C NMR experiments on the α-carbons at natural abundance. However, in practice this abundance is too low to permit relaxation experiments directly on the ^{13}C magnetisation at millimolar peptide concentrations. In order to obtain sufficient sensitivity, ^{13}C was both polarised and detected via the α-protons, as described by Kay et al. (1987) and Nirmala and Wagner (1989).

The ^{13}C relaxation of α-carbons in peptides and proteins is well defined. The dipolar relaxation,

---

Abbreviations: NPY, neuropeptide Y; P7, [A^{15},desY^{21}-L^{24}]NPY(13–36)-amide; IC_{50}, concentration of competitive inhibitor that inhibits 50 percent of the binding of a radioligand to a receptor; CD, circular dichroism; NOE, nuclear Overhauser enhancement; NOESY, NOE spectroscopy; DQF-COSY, double-quantum-filtered correlated spectroscopy; TOCSY, total correlation spectroscopy; HSQC, heteronuclear single-quantum coherence spectroscopy; HSQC-HOHAHA, HSQC-homonuclear Hartmann–Hahn spectroscopy; {^1H}-^{13}C, saturation of protons causing steady-state NOE on carbons; INEPT, insensitive nuclei enhanced by polarisation transfer; DANTE, delays alternating with nutations for tailored excitation; WALTZ-16, wideband, alternating phase, low-power technique for zero residual splitting; FID, free induction decay; 1D, 2D, 3D, one-, two-, three-dimensional; ppm, parts per million; ppb, parts per billion; TSPA, 3-trimethylsilyl-[3,3,2,2-D]-propionic acid; CALIBA, calibration of NOE intensities versus distance constraints; HABAS, program for obtaining stereospecific assignments for α- and β-protons in proteins; DIANA, distance geometry algorithm for NMR applications; REDAC, redundant dihedral angle constraints.

caused by the directly bound $C^{\alpha}H$ proton at a distance of 1.09 Å from the carbon, strongly dominates. The next neighbours to be taken into account for the relaxation of the α-carbons are the intra-residual NH and $C^{\beta}H$ protons. The influence on the relaxation rates of the $^{13}C^{\alpha}$ from all indirectly bound protons in the neighbourhood is of the order of 1%, and their effect can thus be neglected. Hence, the ^{13}C relaxation rate of a C^{α} carbon is a function of the spectral densities of the reorientational motion of the vector along the C^{α}-H^{α} bond. For a structured peptide, these relaxation rates are mainly influenced by the overall molecular tumbling. In the regime of slow rotational motion, i.e., at a magnetic field of 9.4 T and for rotational correlation times $\tau_R > 1$ ns, the ratio between the spin-spin relaxation rate R_2 and the spin-lattice relaxation rate R_1 increases rapidly with increasing τ_R. Assuming a single correlation time, apparent τ_R values were obtained from the R_2/R_1 ratios. Experiments were performed using both 1D and 2D NMR techniques. From the 1D NMR spectra, average behaviour over all residues was calculated, whereas information on residue-specific dynamics was obtained from the 2D data sets.

MATERIALS AND METHODS

Peptide synthesis and purification

Using the *tert*-butyloxycarbonyl (*tert*-BOC) solid-phase technique, the peptide was manually synthesised in a stepwise manner on a 0.2-mmole scale. The *tert*-BOC amino acids used were coupled to *p*-methylbenzhydrylamine resin as 1-hydroxybenzotriazole (HOBt) esters or as activated residues with diisopropylcarbodiimide (DIPCDI), using a two times excess of activated amino acid. The peptide was deprotected with 50/50 (v/v) trifluoroacetic acid/dichloromethane, cleaved from the resin with hydrogen fluoride, and purified applying high performance liquid chromatography (HPLC) on a reversed phase C_{18} column (218TP152022, Vydac). The purity of the peptide was checked by analytical HPLC (C_{18} column 218TP54, Vydac). The experimental molecular weight of 2490.8 Da, determined using a plasma desorption mass spectrometer (Model Bioion 20, Applied Biosystems), was found to agree well with the theoretical molecular weight of 2488.4 Da.

Circular dichroism

CD measurements were performed on a Jasco J-720 spectropolarimeter at 15 and 28 °C, as previously described (Arvidsson et al., 1993). The samples were prepared in H_2O with 20 mM acetic acid (HAc) in 0, 10, 20, 30 and 40% (v/v) 1,1,1,3,3,3-hexafluoro-2-propanol. The peptide concentration was determined by UV light absorption, using a specific absorptivity $\varepsilon_{274.8\ nm} = 4215\ L\ mol^{-1}\ cm^{-1}$, calculated for a peptide containing three tyrosine residues with the tabulated extinction coefficient for the free amino acid in aqueous solution (Sober, 1970).

NMR spectroscopy

Sample preparation. The NMR sample was prepared by dissolving lyophilised material in 20 mM deuterated acetic acid in H_2O, with 30% (v/v) deuterated 1,1,1,3,3,3-hexafluoro-2-propanol and 10% (v/v) D_2O. The sodium salt of 3-trimethylsilyl-[3,3,2,2-D]-propionic acid (TSPA) was used as internal chemical-shift reference (0.25 mM). The peptide concentration was about 6 mM and the uncorrected pH was measured to be 2.7. For the backbone amide proton exchange study, a similar sample was prepared by dissolving the same peptide after

lyophilisation in 70% D_2O and 30% (v/v) 1,1,1,3,3,3-hexafluoro-2-propanol, at pH 3.1, uncorrected reading.

NMR experiments. All 2D NMR spectra were collected in the pure phase absorption mode (States et al., 1982) on a JEOL JNM-A400, if not otherwise stated. Homo- and heteronuclear NMR spectra were recorded at 15 and 28 °C, respectively. The spectral width in the proton dimension was 5 kHz. The numbers of data points reported are complex in the t_2 dimension and hypercomplex in the t_1 dimension. Solvent signal suppression was achieved by continuous-wave presaturation using the decoupler, or by means of an on-resonance DANTE pulse using the transmitter (Zuiderweg et al., 1986). For polarisation transfer in the INEPT sequence, the delay was set to 1.67 ms, which is slightly less than $1/(4J_{CH})$.

^1H NMR experiments for assignment and structure determination. 2D DQF-COSY and NOESY experiments (the latter with a mixing time of 150 ms) were recorded on a JEOL GX-400 at 15 °C. This temperature was found to optimise the intensity and resolution of NOESY cross peaks. The following parameters were used: 96 added FIDs after four dummy scans, 256 and 2048 (DQF-COSY) or 1024 (NOESY) data points in the t_1 and t_2 dimensions, respectively, and a recycle delay of 1.5 s.

The $^3J_{HN\alpha}$ spin-spin coupling constants were determined from extracted 1D slices in the ω_2 dimension through each resolved antiphase cross peak in the DQF-COSY experiment, as described by Arvidsson et al. (1994). The final digital resolution was 0.62 Hz/point in the ω_2 dimension. A double Lorentzian antiphase model, taking into account the baseline offset and slope, was fitted to each extracted slice.

The temperature dependences of the backbone amide proton resonances were determined from a series of 2D TOCSY experiments recorded as described below, in steps of 5 °C over the range 15–50 °C.

The amide proton exchange rates were determined from a series of 2D TOCSY experiments, each accumulated within 25 min with the following parameters: four added FIDs, 200 and 2048 data points in the t_1 and t_2 dimensions, respectively, 30 ms mixing time, a recycle delay of 0.8 s and no dummy scans. The first experiment was started 11.5 min after dissolving the peptide in the D_2O-containing solvent.

In order to assign the ^{13}C resonances, ^1H-^{13}C 2D HSQC and HSQC-HOHAHA spectra (Otting and Wüthrich, 1988) were recorded, with a 30 ms mixing time in the HOHAHA part and a spectral width of 8 kHz in the carbon dimension. These spectra were accumulated with 32 dummy scans, 128 added FIDs, 1024 points in the proton dimension and 128 points in the carbon dimension, centred on the water resonance and at 35 ppm, respectively. A recycle delay of 1.5 s was used.

NMR experiments for determination of ^{13}C relaxation. The pulse sequences used in the NMR experiments to determine the spin-spin and spin-lattice ^{13}C relaxation rates and the $\{^1H\}$-^{13}C NOEs, were those described by Barbato et al. (1992) with some minor alterations. In all three types of experiment a total recycle delay of 4 s was used, the water signal was additionally suppressed by an on-resonance DANTE presaturation of 1.5 s, and carbon decoupling was performed by applying WALTZ-16 (Shaka et al., 1983) during acquisition. The spin-spin relaxation experiments were recorded with a 2 ms time delay between refocusing pulses, in order to minimise the build-up of antiphase magnetisation (Peng et al., 1991). The ^{13}C spectra for determination of the NOEs were accumulated on a Varian Unity 500 spectrometer in order to improve sensitivity.

In the 1D spin-spin relaxation rate measurements, spectra were recorded applying seven time delays: 8, 16, 32, 48, 60, 96 and 128 ms. In the corresponding spin-lattice relaxation rate measurements, spectra with delays of 20, 100, 200, 300, 400 and 500 ms were accumulated. With 512 FIDs added for each time delay and using 2048 data points, it took circa 8 h to collect both series of data. The data sets were acquired at several temperatures from 10 to 45 °C.

In the 2D relaxation experiments, a spectral width of 2.2 kHz was used in the ^{13}C dimension. Spectra were acquired with 512 and 56 data points in the proton and carbon dimension, respectively. The acquisition of 96 added FIDs and 16 dummy scans, took circa 12 h per time delay. The 2D spin-spin relaxation experiments were acquired with time delays of 4, 12, 24, 40 and 60 ms. In the 2D spin-lattice relaxation experiments, time delays of 10, 105, 205, 305 and 405 ms were used. A complete 2D data set for determination of ^{13}C spin-spin and spin-lattice relaxation rates required circa 120 h. These experiments were performed at 28 °C, found to be a suitable compromise considering temperature stability, line width and sensitivity.

Structure calculations

Distance restraints. The intensity of each NOE cross peak in the NOESY spectrum obtained with 150 ms mixing time was determined by integration using the FELIX software (Biosym Technologies, Inc.). The intensities were converted into upper limit distances by applying CALIBA (Güntert et al., 1991a,b), using three different calibration curves, i.e., relationships between cross-peak intensity and upper limit distance.

Dihedral angle restraints. The ϕ dihedral angle restraints were calculated from the $^3J_{HN^\alpha}$ spin-spin coupling constants using HABAS (Güntert et al., 1989).

Structure calculation using DIANA. The P7 structures were calculated as described by Arvidsson et al. (1993). Initially, 50 structures were generated by DIANA including the REDAC routine, which improves the convergence of the structure calculations by introducing redundant dihedral angle restraints. The 10 structures with lowest target function values were chosen for further refinement.

Structure refinement by rEM. The 10 refined DIANA structures were energy minimised twice, each time with 500 conjugate gradient iterations, employing the AMBER force field (Weiner et al., 1984) in vacuum. The distance restraint force constant was increased from 1 to 2 kcal mol^{-1} $Å^{-2}$ between the two rEM stages, while the ϕ dihedral angle restraint force constant was 5 kcal mol^{-1} rad^{-2} throughout. The ω dihedral angles were restrained to $\pm$ 180°, using a force constant of 20 kcal mol^{-1} rad^{-2}. Other details of the structure refinement protocol were as previously described (Arvidsson et al., 1993).

Calculation of the ^{13}C relaxation rates

In the 1D ^{13}C relaxation rate experiments, the intensities were determined by integrating over all H^α resonances in the inverse detected spectra. From the 2D spectra, residue-specific cross-peak intensities were determined from extracted 1D slices along the ω_2 dimension. All time series of intensities, consisting either of averaged 1D data or of residue-specific 2D data, were fitted with single exponential two-parameter decays, $I(t) = I_o \cdot \exp(-t \cdot R_{1,2})$, using a nonlinear least-square minimisation routine. Of course, in reality the decay curves of the 1D experiments are multiexponential, but no attempt was made to resolve them.

Determination of the overall rotational correlation time

The ratio of the ^{13}C dipolar transverse and longitudinal relaxation rates (Abragam, 1962; Lipari and Szabo, 1982) of α-carbons was used to estimate the overall rotational correlation time τ_R:

$$\left(\frac{R_2}{R_1}\right)^{DD} = \frac{1}{2} \cdot \frac{4J(0) + 3J(\omega_C) + J(\omega_H - \omega_C) + 6J(\omega_H) + 6J(\omega_H + \omega_C)}{3J(\omega_C) + J(\omega_H - \omega_C) + 6J(\omega_H + \omega_C)} \quad (1)$$

where

$$J(\omega) = \frac{2}{5} \cdot \frac{\tau_R}{1 + (\omega\tau_R)^2} \quad (2)$$

Here it is assumed that the molecule has a spherical shape and that the rotational diffusion is described by a single correlation time, i.e. $D_R = 1/6\tau_R$. In the fast-motion regime, where $J(\omega) \propto \tau_R$, this ratio equals unity. In the slow-motion regime, where $J(\omega) \propto 1/(\omega^2\tau_R)$ for $\omega \neq 0$, this ratio is proportional to τ_R^2. The overall rotational correlation time τ_R was calculated from the measured R_2/R_1 ratio using Eqs. 1 and 2. The advantages in using the ratio of the relaxation rates rather than a single rate, e.g. R_2, for determination of τ_R, are that any uncertainty in the C^α-H^α distance is eliminated and that effects of local motion are partly cancelled out. The ratio of ^{13}C relaxation rates has until now not been widely used in practise, because it is unity for small molecules and has not been experimentally accessible for larger molecules, due to low sensitivity of ^{13}C NMR. For peptides this method will be useful for rotational correlation times from circa 1 ns, where the ratio R_2/R_1 starts to deviate from unity, and upwards, until the increase of transverse relaxation rate deteriorates resolution and sensitivity.

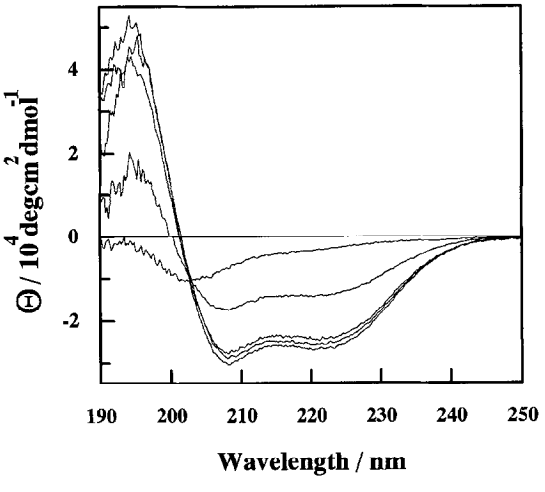

Fig. 1. CD spectra of P7 recorded at 15 °C, in 20 mM HAc with different mixtures of H_2O and 1,1,1,3,3,3-hexafluoro-2-propanol. At 222 nm, counting downwards from the top, they are valid for 0, 10, 40, 20 and 30% (v/v) cosolvent. The peptide concentration was initially 53 μM at 0% cosolvent. The data were corrected for dilution effects resulting from addition of cosolvent. All spectra were recorded using a 2 mm path length.

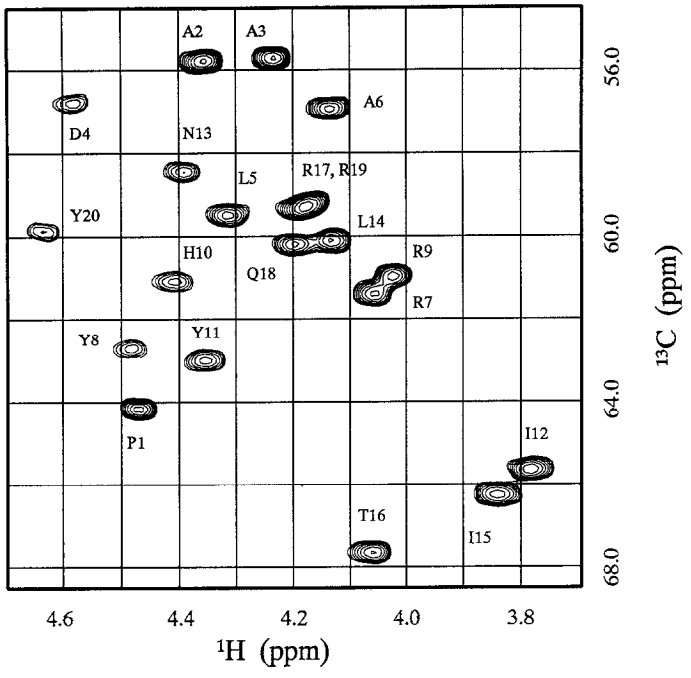

Fig. 2. The C^{α}-H^{α} region of a 2D heteronuclear single-quantum coherence (HSQC) spectrum of P7 recorded at 28 °C. This experiment was accumulated with 128 t_1 data points and 1024 points in the t_2 dimension, using spectral widths of 8 and 5 kHz in the carbon and proton dimension, respectively. All residues display well-separated cross peaks, except Arg^{17} and Arg^{19}, which have practically coinciding chemical shifts.

RESULTS

Circular dichroism

Circular dichroism spectra of P7, recorded in different concentrations of 1,1,1,3,3,3-hexafluoro-2-propanol in 20 mM HAc at 15 °C, are shown in Fig. 1. A well-defined isodichroic point at 203 nm in the CD spectra justifies a two-state secondary structure model, with an equilibrium between configurations with mainly α-helix and mainly random coil. At 15 °C, the negative ellipticity above 203 nm is largest at 30% (v/v) 1,1,1,3,3,3-hexafluoro-2-propanol, whereas at 28 °C the CD spectra of P7 practically coincide for the cosolvent concentrations from 20 to 40% (v/v) (data not shown). Taking the ellipticity at 222 nm as a measure of α-helix content, and using mean residual contributions of −35 700 deg cm^2 $dmol^{-1}$ for α-helix and 3900 deg cm^2 $dmol^{-1}$ for random coil (Greenfield and Fasman, 1969), we calculated that the peptide P7 forms α-helix up to 75 and 66% at 15 and 28 °C, respectively. This corresponds to α-helical conformations consisting of 15 and 13 residues, respectively.

NMR spectroscopy

Assignments and chemical shifts. The proton resonance assignments were straightforward to make from the 2D homonuclear spectra at 15 °C, using standard procedures (Wüthrich, 1986). The assignments of the $^{13}C^{\alpha}$ resonances were made from the 2D heteronuclear ^{13}C-^1H correlation

spectra at 28 °C, and by comparison with the proton chemical shifts at lower temperature. The temperature change from 15 to 28 °C caused the $C^{\alpha}H$ proton resonances to shift downfield by less than 0.04 ppm. In the 2D heteronuclear ^{13}C-^{1}H correlation spectrum shown in fig. 2, all C^{α}/H^{α} cross peaks were resolved, except for those of Arg^{17} and Arg^{19} which have practically coinciding shifts in both dimensions at 28 °C. The shifts of the $^{13}C^{\alpha}$ resonances at 28 °C and the proton resonances at 15 °C are compiled in Table 1, together with the spin-spin coupling constants $^{3}J_{HN\alpha}$.

The secondary chemical shifts for $C^{\alpha}H$ protons and C^{α} carbons, relative to their random-coil values (Richarz and Wüthrich, 1978; Wüthrich, 1986), have been calculated and are plotted in Fig. 3. To suppress local fluctuations, a mean secondary shift over three residues is plotted for each residue. It should be noted that the secondary chemical shifts for both the upfield shifted proton resonances and the downfield shifted carbon resonances have been plotted as positive, in order to simplify comparison. These shifts suggest that the peptide has a well-defined central α-helix. The larger secondary chemical shifts in the C-terminal part of the peptide, particularly clear for the $C^{\alpha}H$ protons, indicate that this section might be more stable as compared with the N-terminal part.

TABLE 1
NMR CHEMICAL SHIFTS AND $^{3}J_{HN\alpha}$ SPIN-SPIN COUPLING CONSTANTS OF P7[a]

Residue	Chemical shift (ppm)						$^{3}J_{HN\alpha}$ coupling constant (Hz)
	$^{13}C^{\alpha}$	NH	$C^{\alpha}H$	$C^{\beta}H$	$C^{\gamma}H$	Other	
Pro^{1}	64.2		4.47	2.20,2.61	2.17	3.48,3.58 (H^{δ})	
Ala^{2}	55.7	8.76	4.33	1.54			4.6
Ala^{3}	55.7	8.25	4.21	1.47			3.9
Asp^{4}	56.7	8.04	4.56	2.92			5.1
Leu^{5}	59.4	7.64	4.32	1.84	1.75	0.98,1.06 (H^{δ})	5.3
Ala^{6}	56.8	8.00	4.14	1.56			
Arg^{7}	61.4	8.00	4.05	1.96,1.98	1.57	3.23(H^{δ}); 7.05(H^{ε})	5.4
Tyr^{8}	62.9	8.15	4.47	3.28		7.16(H^{δ}); 6.86(H^{ε})	5.0
Arg^{9}	60.9	8.66	4.02	2.02,1.90	1.78	3.20(H^{δ}); 7.15(H^{ε})	4.2
His^{10}	61.1	8.20	4.39	3.44		8.46(H^{δ}); 7.14(H^{ε})	5.8
Tyr^{11}	63.0	8.39	4.34	3.29		7.12(H^{δ}); 6.84(H^{ε})	5.5
Ile^{12}	65.6	8.61	3.76	1.93,1.53	1.27	0.92(H^{δ}); 0.79(H^{ε})	3.9
Asn^{13}	58.4	8.12	4.38	2.82,3.04		6.63,7.47(H^{δ})	5.9
Leu^{14}	60.1	7.99	4.12	1.90	1.65	0.91(H^{δ})	
Ile^{15}	66.3	8.53	3.81	1.86	1.16,1.48	0.86(H^{δ}); 0.74(H^{ε})	5.3
Thr^{16}	67.7	8.17	4.03	4.42	1.39		6.0
Arg^{17}	59.3	7.95	4.17	2.05,1.86	1.78	3.21(H^{δ}); 7.24(H^{ε})	4.6
Gln^{18}	60.1	8.20	4.16	2.23	2.50	6.49,7.01(H^{ε})	5.4
Arg^{19}	59.3	8.17	4.14	1.72,1.77	1.39	3.01,3.08(H^{δ}); 7.04(H^{ε})	5.8
Tyr^{20}	59.9	8.06	4.62	2.96,3.28		7.28(H^{δ}); 6.87(H^{ε})	7.7
NH_2		7.00,7.36					

[a] Chemical shifts and coupling constants were recorded in 20 mM HAc in H_2O with 30% (v/v) 1,1,1,3,3,3-hexafluoro-2-propanol for $^{13}C^{\alpha}$ resonances at 28 °C, proton resonances at 15 °C. All chemical shifts are referenced relative to internal TSPA.

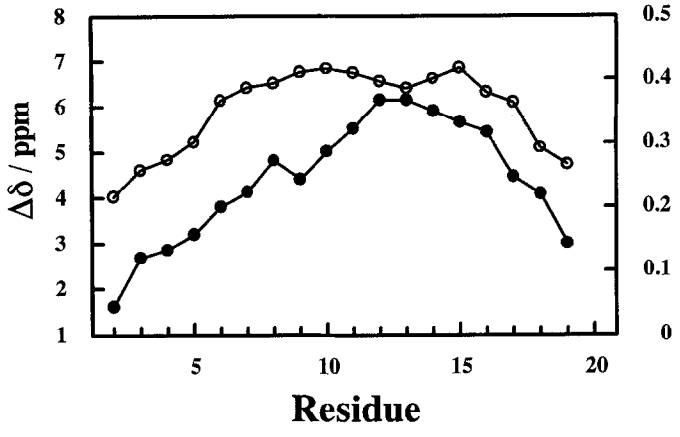

Fig. 3. Secondary chemical shifts of the $C^{\alpha}H$ protons and the C^{α} carbons of P7 recorded at 15 and 28 °C, respectively. The secondary shifts of protons and carbons are plotted with closed and open circles and the values are given on the right and left vertical axis, respectively. The secondary shifts have been calculated relative to the random coil values for protons and carbons reported by Wüthrich (1986) and Richarz and Wüthrich (1978), respectively. Note that the shifts are plotted as positive for upfield shifted proton resonances and downfield shifted carbon resonances. All shifts have been averaged over three residues, in order to suppress local fluctuations. All chemical shifts are referenced to internal TSPA.

Analysis of structurally important NOE intensities and spin-spin coupling constants. The NOE intensities with bearing on the secondary structure are indicated in Fig. 4. Extensive medium-range $d_{\alpha N}(i,i+3)$ and $d_{\alpha\beta}(i,i+3)$ NOE connectivities in the whole range from Ala^{3} to Arg^{19}, in

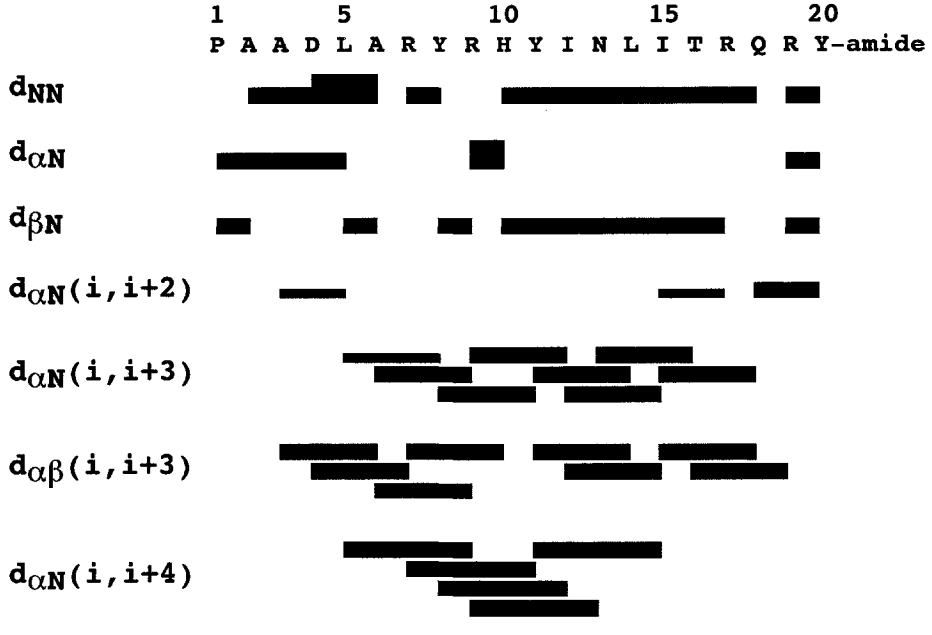

Fig. 4. Amino acid sequence of P7 and survey of the NOE connectivities important for the secondary structure of P7 in 30% (v/v) 1,1,1,3,3,3-hexafluoro-2-propanol. Thick, medium and thin bars indicate NOEs with high, medium and low intensity, respectively. The NOE data were recorded at 15 °C.

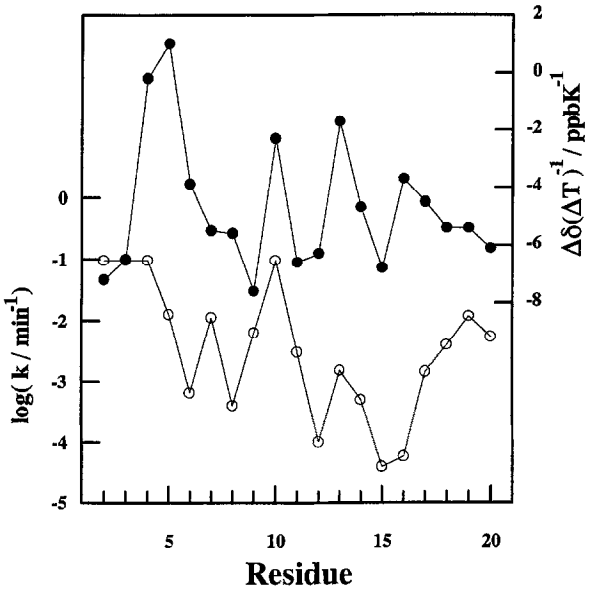

Fig. 5. Exchange rates of backbone amide protons of P7, and the temperature dependences of their chemical shifts. Open circles: the first-order rate constants of the exchange kinetics, with vertical scale to the left. The accumulation of the exchange data started 11.5 min after dissolving the peptide in a solvent containing 70% (v/v) D_2O with 20 mM deuterated acetic acid and 30% (v/v) 1,1,1,3,3,3-hexafluoro-2-propanol. Uncorrected pH reading was 3.1. The exchange rates of the amide protons of Ala^2-Asp^4 and His^{10} were too high to be measured in this experiment, and their exchange rates plotted are thus lower limits. Closed circles: the temperature dependences of the amide proton resonances, with vertical scale to the right, determined from spectra recorded at 15–50 °C.

addition to five $d_{\alpha N}(i,i+4)$ connectivities within a part of the same region, i.e. Leu^5 to Ile^{15}, suggest that almost the entire peptide is engaged in an α-helical conformation. A large number of d_{NN} NOEs from Ala^2 to Tyr^{20} confirm this type of secondary structure. The $^3J_{HN\alpha}$ spin-spin coupling constants of P7 have been included in Table 1. These values, except for that of the terminal Tyr^{20}, all fall below 6 Hz, in agreement with an overall helical structure of the peptide.

Backbone amide proton exchange. The backbone amide proton exchange rates of P7, recorded at 15 °C, are plotted in Fig. 5. For the four N-terminal amino acid residues and for His^{10} the amide protons had already exchanged completely before the first measurement. Hence, these protons have exchange rate constants of at least 0.1 min^{-1}. For all other residues the rate constants were smaller than 0.01 min^{-1}. The residues Ile^{12}, Ile^{15} and Thr^{16} show the lowest exchange rates, with $k_{ex}<10^{-4}$ min^{-1}, a reduction of the exchange rate with more than three orders of magnitude compared to the amide protons in the first four residues and in His^{10}. The reduced exchange rates suggest that most amide protons of the sequence Leu^5-Tyr^{20} are involved in hydrogen bonds.

Temperature dependences of chemical shifts of backbone amide proton resonances. The chemical shifts of the amide proton resonances were all found to change linearly with temperature within the temperature region studied, i.e. 15–50 °C. The chemical-shift change per degree of temperature change is plotted in Fig. 5. The temperature dependences are particularly small for the residues Asp^4, Leu^5, His^{10} and Asn^{13}, which all have dependences between +1 and −2 ppb K^{-1}. The chemical shifts of all other amide protons change upfield with increasing temperature, with

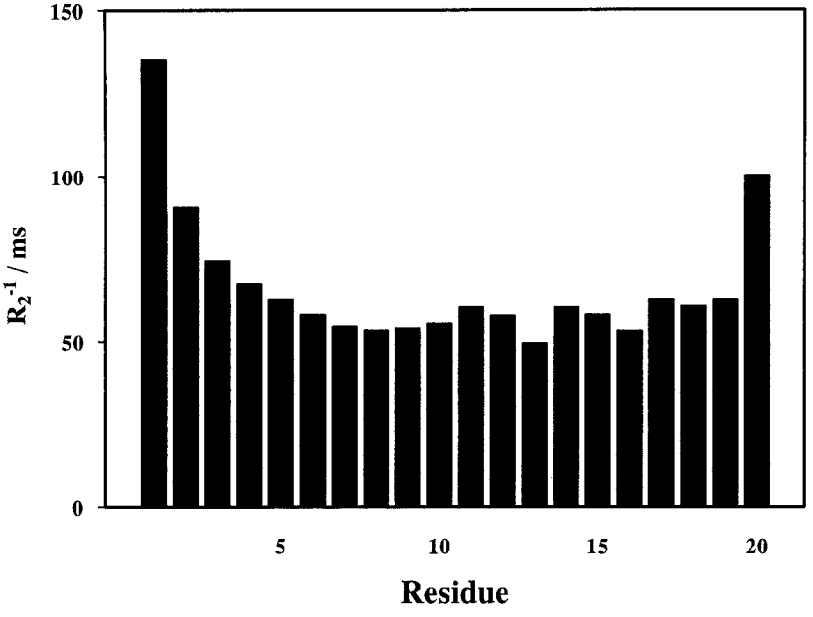

Fig. 6. ^{13}C spin-spin relaxation times, $T_2 = R_2^{-1}$, of the α-carbons in P7, recorded at 28 °C. The spin-spin relaxation experiments were accumulated with time delays of 4, 12, 24, 40 and 60 ms. The plotted data represent the average of two experiments.

linear slopes ≤ -3 ppb K^{-1}. Residues Ala^2, Ala^3, Arg^9, Tyr^{11}, Ile^{12} and Ile^{15} all have large temperature dependences, with slopes < -6 ppb K^{-1}.

^{13}C spin-lattice and spin-spin relaxation rates. In the 1D experiments, unresolved averages of the relaxation rates of all $^{13}C^{\alpha}$ carbons were determined. For the spin-lattice relaxation rate we obtained the average value $R_{1,av} = 3.70\ s^{-1}$, and the spin-spin relaxation rate $R_{2,av} = 14.7\ s^{-1}$ at 28 °C.

In the 2D experiments, residue-specific $^{13}C^{\alpha}$ relaxation rates were determined for all residues, except for Arg^{17} and Arg^{19} which could not be resolved individually, see Fig. 2. The latter have been assigned identical R_1 and R_2 values. The ^{13}C spin-lattice relaxation rates R_1 for the α-carbons, except for those of Pro^1 and Tyr^{20}, were found to be rather uniform over the peptide sequence, having random variations around 3.81 s^{-1} (data not shown). In Fig. 6 the inverse rate R_2^{-1} has been plotted instead of R_2, in order to facilitate visual comparison with the spread of the structures in Fig. 7 and the calculated rmsd values shown in Fig. 8. The data demonstrate that the entire section Leu^5-Arg^{19} has α-carbons with uniform R_2 values, spread about an average of 17.3 s^{-1}. The four N-terminal residues, Pro^1-Asp^4, show decreasing ^{13}C spin-spin relaxation rates of the α-carbons on going towards the terminus. Also the C-terminal Tyr^{20} shows a low R_2 value.

Proton-detected ^{13}C NOE spectroscopy. The signal-to-noise ratio in these experiments was not sufficient to permit reliable quantification of the $\{^1H\}$-^{13}C NOEs, even at 500 MHz. Nevertheless, the NOEs of the first three N-terminal residues were significantly larger than for the rest of the molecule (data not shown).

Structural analysis

Overall conformation of structures. An overview of the restraints used in the structure calcula-

Fig. 7. Stereoview of 10 superimposed structures of P7, calculated from NMR-derived distance and angle restraints. The superposition was made by minimising the rmsd of C', C^{α} and N over residues 8–16. The N-terminus is shown at the top.

tions and the violations of the final structures is presented in Table 2. The 10 solution structures of P7, calculated from NMR-derived restraints, have been superimposed on each other and are presented in a stereoview, Fig. 7, with the N-terminus at the top. It is clearly seen that the α-helix is well defined in the central part of the peptide. The superimposed structures have a wider spread in the N-terminal section than in the C-terminal part. Minimised local rmsd values were calculated for C', C^{α} and N of all tripeptides along the sequence, for all possible combinations of pairs of

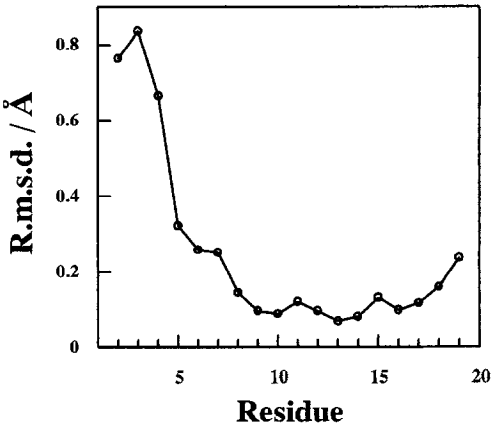

Fig. 8. Minimised local rmsd of the C', C^{α} and N of all tripeptides along the primary structure, plotted at the position of the central residues of P7. The indicated values are average values of the 45 pairwise comparisons among the 10 structures.

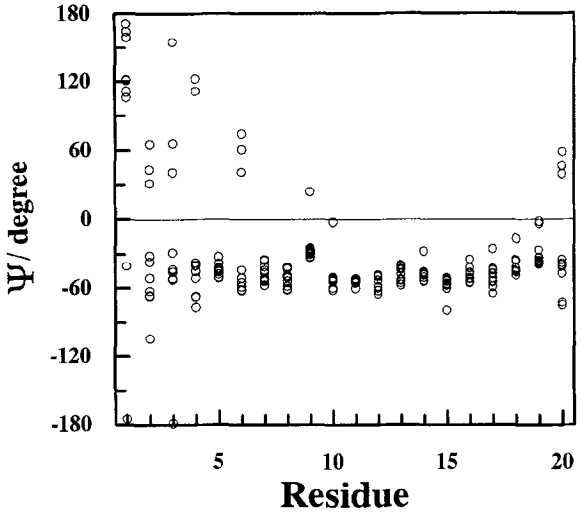

Fig. 9. Backbone dihedral angles ψ in the 10 calculated structures of P7.

the 10 structures. In each case the rmsd was taken to represent the central residue of the tripeptide, and averages over all the 45 combinations of pairs were calculated. These averages are shown in Fig. 8. The small rmsd values over the range Tyr^{8}-Gln^{18} reveal that the sequence Arg^{7}-Arg^{19} has a particularly well defined conformation. In contrast, the conformation of the N-terminal sequence Pro^{1}-Asp^{4} stands out as being ill defined.

TABLE 2
OVERVIEW OF RESTRAINTS USED IN THE STRUCTURE CALCULATIONS AND VIOLATIONS OF THE FINAL STRUCTURES

NOE restraint violations[a]	
Number >0.1 Å	25.6 (21–35)
Sum (Å)	8.45 (6.41–12.44)
Maximum (Å)	0.93 (0.64–1.38)
NOE restraints[b]	
Total	216
Intraresidual	95
Sequential	61
Medium range[c]	60
Dihedral angle restraints	
ϕ[d]	15
ψ[e]	11
χ^{1}[e]	5

[a] Average among the 10 structures and range (in parentheses).
[b] NOE restraints calibrated by CALIBA and retained by DIANA as nonredundant.
[c] Sum of number of NOEs over three, four and five residues.
[d] Based on 15 determined $^{3}J_{HN\alpha}$ spin-spin coupling constants, using HABAS.
[e] Based on NOEs and $^{3}J_{HN\alpha}$ spin-spin coupling constants, using HABAS.

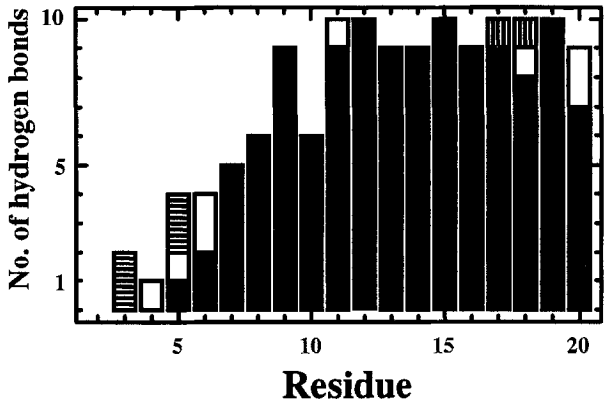

Fig. 10. The number of detected backbone hydrogen bonds in the 10 P7 structures. Filled and unfilled boxes indicate NH(i)–CO(i−4) and NH(i)–CO(i−3) hydrogen bonds, respectively. Horizontally and vertically hatched boxes denote NH(i)–CO(i−2) and NH(i)–CO(i−5) hydrogen bonds, respectively.

Backbone dihedral angles ϕ and ψ. In Fig. 9 the dihedral angles ψ in the 10 structures of P7 have been plotted. All amino acid residues, except the first four and the C-terminal Tyr^{20}, have ψ angles that agree very well with an ideal α-helix. The dihedral angles ϕ in the P7 structures show an even better defined ideal α-helix in the central region and a similar spread in the terminal sections (data not shown).

Backbone hydrogen bonds. The backbone hydrogen bonds detected in the 10 structures of P7 are indicated in Fig. 10. All hydrogen bonds included fulfil the criteria described earlier by Arvidsson et al. (1993). The large number of (i,i−4) hydrogen bonds between Leu^5 and Arg^{19} is an indicator of a stable α-helix in that region.

DISCUSSION

Peptide structure

From the CD results we deduce that at 15 and 28 °C, out of the 20 amino acid residues of P7, on average 15 and 13 residues, respectively, are in α-helix conformation. This agrees well with what can be observed by visual inspection of the superimposed NMR structures in Fig. 7, and more quantitatively verified by data deduced from the structures, such as the dihedral angles ψ of Fig. 9 and the hydrogen bonds indicated in Fig. 10. Both these sets of data, at 15 °C, show that residues Leu^5-Arg^{19}, i.e. altogether 15 residues, are in α-helix conformation, whereas the N-terminal sequence Pro^1-Asp^4 and the C-terminal residue Tyr^{20} do not conform well to a defined secondary structure. The local rmsd values of Fig. 8 underscore that the structure of the first four residues is ill defined in comparison with the rest of the molecule. If the limit for a well-defined structure in Fig. 8 is taken at an rmsd of 0.35 Å, there is complete agreement with the results of the analyses of dihedral angles ψ and hydrogen bonds.

When the temperature is changed from 15 to 28 °C, only a few of the $C^{\alpha}H$ proton resonances of P7 in the C-terminal region are shifted downfield, by 0.02 to 0.035 ppm. This suggests a gradual and limited uncoiling of the helix from the C-terminal end. A similar effect was recently observed

(Arvidsson et al., 1993) for another peptide, M32, which is 25 amino acid residues long and has the same 12-residue C-terminal part as P7.

The results presented in Fig. 5 show that in the centre of the peptide, a strong correlation occurs between the exchange rates of the amide protons and the temperature dependence of their chemical shifts. The chemical shifts of rapidly exchanging amide protons have small temperature dependence, and vice versa. This correlation is different from that inferred by Dyson et al. (1988) in their work on shorter peptides with tendency to form β-turns, where the decrease in exchange rates due to hydrogen-bond formation corresponded to a decrease of the temperature dependence of the chemical shift. The latter investigations were performed on peptides in pure aqueous solutions at pH 4.1, whereas in the present work we have used a mixed solvent, with 30% (v/v) of 1,1,1,3,3,3-hexafluoro-2-propanol at pH 3.1. We have found that in this solvent, peptide P7 forms a well-defined amphipathic α-helix. On the hydrophilic side of this helix, the amide protons display fast exchange and relatively small temperature dependence of the chemical shifts. On the hydrophobic side the properties are reversed, with slowly exchanging amide protons and larger temperature dependence of the chemical shifts. The difference in amide proton exchange rates between the two sides of the helix is probably to a large extent caused by different exposure to water. In an α-helix of a peptide like P7, the water accessibility to the backbone amide protons should be governed by the nature of the side chains and their solvation. On the hydrophilic side, solvation should occur to a large extent by water, whereas on the hydrophobic side, solvation by the cosolvent 1,1,1,3,3,3-hexafluoro-2-propanol might dominate and prevent the water from reaching the amide protons. Such a solvation by the cosolvent molecules is also expected to be an effective mechanism for their stabilising effect on the structure of the amphipathic α-helix.

The 12-residue sequence Arg^{9}-Tyr^{20} of P7 is identical to the sequence Arg^{14}-Tyr^{25} of the two galanin–NPY chimeras M32 and M88, i.e. galanin(1–12)-Pro-NPY(25–36)amide and galanin(1–12)-Ala-NPY(25–36)amide, respectively, for which the exchange rates of the amide protons were reported recently (Arvidsson et al., 1994). The measured exchange rates of the amide protons of these parts of M32 and M88 nearly coincide with those of the corresponding residues of P7 shown in Fig. 5.

The linear temperature dependence, observed for all amide proton chemical shifts of P7, indicates that the overall stability of the α-helical structure changes only gradually, and no melting of the secondary structure occurs within the temperature range 15–50 °C. This behaviour and the small and gradual temperature-induced uncoiling of P7 from the C-terminus, deduced from the temperature dependence of the chemical shifts of the $C^{\alpha}H$ proton resonances, vide supra, show that the α-helix of P7 is quite stable. This is in full agreement with the CD results. It may thus be concluded that the secondary structure of P7 is essentially unchanged when the temperature is changed from 15 to 28 °C. Any changes of the α-helical structure are distributed over several residues. Hence, the ^{13}C relaxation results obtained at 28 °C are valid for a peptide structure which differs only slightly from that determined at 15 °C.

Peptide dynamics, aggregation and solvation

From the 1D experiments, the average $^{13}C^{\alpha}$ relaxation rates were determined to be $R_{1,av} = 3.7$ s^{-1} and $R_{2,av} = 14.7$ s^{-1}. The ratio $R_{2,av}/R_{1,av} = 3.97$, which by fitting with Eqs. 1 and 2 was found to correspond to $\tau_{R,av} = 3.5$ ns at 28 °C.

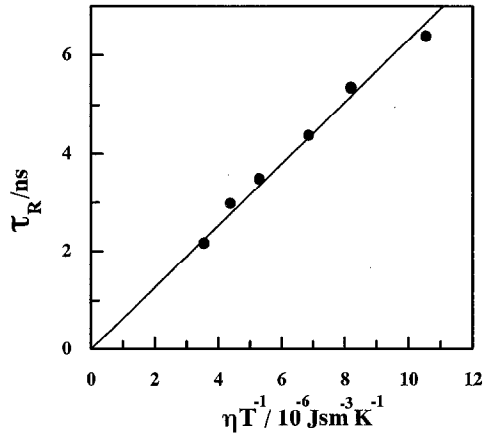

Fig. 11. Overall rotational correlation times plotted against the product of viscosity and the inverse temperature. These correlation times have been calculated from the R_2/R_1 ratios obtained in 1D experiments at several temperatures in the range 8.5–45 °C. A molecular volume of the peptide was calculated from the slope of the straight line, fitted to the data in this figure.

The overall rotational correlation times at several temperatures were calculated in the same way and are plotted in Fig. 11 as function of the product of the solvent viscosity η and the inverse absolute temperature T^{-1}. The linear dependence shown in the figure fits well with the Stokes–Einstein relationship

$$\tau_R = \frac{V}{k_B} \cdot \frac{\eta}{T} \tag{3}$$

where τ_R is the overall rotational correlation time, V the molecular volume of the peptide, η the viscosity of the medium, k_B Boltzmann's constant and T the absolute temperature. Viscosities for mixtures of the solvent with 30% (v/v) of 1,1,1,3,3,3-hexafluoro-2-propanol at different temperatures were obtained from A. Gräslund (personal communication). From the slope of the line, the effective volume of the molecule is calculated, V_{eff} = 8400 Å^3. The implications of this calculated value will be discussed below.

The 1D and 2D NMR relaxation spectra offer different advantages. The 1D data, analysed by integrating over all α-proton resonances in inverse detection experiments, provide a fast method to determine the overall rotational correlation time, whereas the 2D NMR experiments provide data that contain information on residue-specific relaxation parameters.

The spin-spin relaxation rate R_2 is more sensitive to local dynamics than the longitudinal relaxation rate R_1. R_2 is dominated by the zero-frequency spectral density, which does not affect R_1. As a result, R_2 is very sensitive to slow motion. The large R_2 relaxation rates measured for the central part of the peptide are due to a large zero-frequency spectral density, because the backbone atoms of the stable α-helix, and hence also the C^α-H^α vectors, are bound to follow the overall motion of the molecule. The decrease of R_2 at the termini of the peptide is due to a reduction of this zero-frequency spectral density, caused by an increase of the amplitudes of fast internal motions.

A comparison of the ^{13}C spin-spin relaxation times and the 3D solution structure, determined

from NMR-derived restraints, demonstrates that residues having large ^{13}C relaxation times show large local rmsd values, as seen from Figs. 6 and 8, respectively. This is most evident for the N-terminal residues Pro^{1}-Asp^{4}, but it can also be seen for the C-terminal Tyr^{20}. The local rmsd values calculated for the 10 P7 structures are direct consequences of the set of distance and dihedral angle restraints included in the structure calculations. From the spin-spin relaxation data presented in Fig. 6, it is clear that the N-terminal part of the peptide has a higher mobility, as compared with the central and the C-terminal sections. The relaxation data further demonstrate that the residues in the central part of the peptide, i.e. Leu^{5}-Arg^{19}, all participate in a well-defined and truly stable α-helix.

The overall rotational correlation times were calculated from the experimental data using the R_2 to R_1 ratio (Palmer et al., 1991; Redfield et al., 1992), applying the theoretical expression of this ratio as a function of τ_R, Eq. 1, and assuming a single correlation time, Eq. 2. It can be shown, using the model-free approach (Lipari and Szabo, 1982), that this ratio is to a large extent independent of fast internal motion. The reason for this is that R_1 and R_2 are affected similarly by this motion.

An effective molecular volume of 8400 $Å^3$ was calculated from the slope of the straight line, shown in Fig. 11, using the Stokes–Einstein formula. From the molecular weight and estimated density (1.4 g cm^{-3}) of the peptide, a molecular volume of 2950 $Å^3$ was calculated. The difference between the two calculated molecular volumes should be equal to the solvation volume surrounding the peptide. If this volume difference, 5450 $Å^3$, is transformed into a solvation shell, the thickness of the shell equals 3.7 Å. From the density of 1,1,1,3,3,3-hexafluoro-2-propanol (1.62 g cm^{-3}), the molecular volume of the cosolvent was calculated to be 172 $Å^3$. The corresponding molecular volume for H_2O was calculated similarly to be 30 $Å^3$. Hydration of 0.3–0.4 g H_2O per g protein is needed to account for the hydrodynamic behaviour of a typical globular 30 kDa protein (Cantor and Schimmel, 1980). This corresponds to a hydration shell of 2.8 Å average thickness, i.e., a monolayer of water molecules, which means that each water molecule covers circa 10 $Å^2$ of the surface. The entire surface of P7 is circa 1000 $Å^2$, assuming that P7 has a spherical shape. If we suppose that this surface has to be covered by water and cosolvent molecules, with areas of circa 10 and 25 $Å^2$ per molecule, respectively, then the total volume of these water and cosolvent molecules must equal the solvation volume of 5450 $Å^3$. This problem, which demands that water and cosolvent have to cover simultaneously the entire surface of 1000 $Å^2$ and fill the solvation volume of 5450 $Å^3$, has a single solution for P7 monomers, for which the solvation layer comprises 37 water and 25 cosolvent molecules.

If P7 would form dimers, the solvation volume would be reduced by 2950 $Å^3$, i.e., it would be equal to 2500 $Å^3$. The surface of the dimer aggregate would be the sum of the surfaces of the two monomers, minus the surfaces of interaction between the monomers. This interaction surface is estimated to be 25% or less of the entire surface. For this model of dimers, the two requirements of surface coverage and volume filling cannot be fulfilled simultaneously. Thus, the solvation volume that is calculated for the dimer is too small to permit the formation of a complete layer of solvation over the total surface of the dimer molecule. It can be shown that the interaction surface has to be at least 58% of the entire dimer surface, to satisfy the requirements on surface and volume. Such a large interaction surface is considered to be unrealistic. We conclude that a dimer aggregate does not satisfy our relaxation data. In addition, no intermolecular cross peaks, indicative of P7 dimers, were observed in the NOESY spectrum.

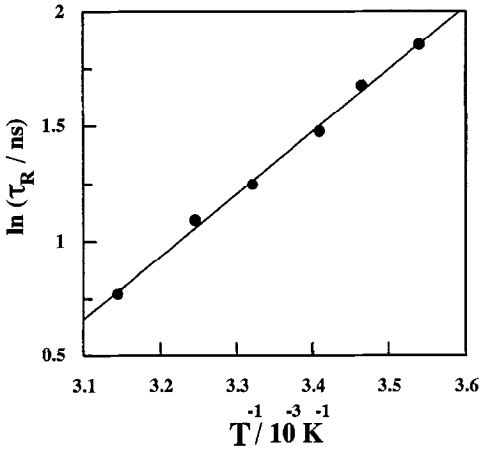

Fig. 12. Natural logarithm of the overall rotational correlation time plotted against the inverse temperature, in the same temperature range as for Fig. 11. Using the Arrhenius relationship, an activation energy of 5.5 kcal mol^{-1} was determined.

In Fig. 12 an Arrhenius plot for the overall rotational correlation time is shown. From the slope of the straight line, plotted for the temperature range of 8.5–45 °C, an activation energy of 5.5 kcal mol^{-1} can be calculated, i.e., close to the value of the viscosity itself. This suggests that both molecular volume and shape of the peptide are unchanged over this temperature range. Both unwinding of the peptide helix, with accompanying increase of solvation, and the formation of dimers would cause an increase of the peptide volume and affect the measured activation energy.

At 28 °C we can compare relaxation data from the 1D and 2D ^{13}C NMR experiments. The 1D experiments give the ratio $r_{av} = R_{2,av}/R_{1,av} = 3.97$. From the residue-specific relaxation rates $R_{1,i}$ and $R_{2,i}$, determined from the 2D experiments, we obtain the residue-specific ratios $r_i = R_{2,i}/R_{1,i}$. The average of r_i over all the residues of P7 gives $r_{i,(1-20)} = 4.16$. However, both these ratios are influenced by the fast local dynamics of the terminal residues Pro^1-Asp^4 and Tyr^{20}. The corresponding values of τ_R are, consequently, smaller than that of the backbone of the more rigid α-helix of the sequence Leu^5-Arg^{19}. For this sequence we calculate the average ratio $r_{i,(5-19)} = 4.46$ and the corresponding $\tau_{R,(5-19)} = 3.76$ ns. This value should be compared with $\tau_R = 3.48$ ns, obtained from the 1D experiments. Thus, in our case, the 1D results underestimate τ_R, and consequently also the effective volume V_{eff}, by almost 8%.

At this point it is also necessary to consider other possible contributions to the 1D spectra than those of α-carbons with a single covalently bound hydrogen. The refocused INEPT steps in our pulse sequences suppress the response of A_2X spin systems, e.g. of glycine residues, not present in P7, whereas that of the AX spin system $C^\beta H$ of Thr^{16} passes the editing filter and contributes to the 1D spectra. From the 2D experiments we calculate for Thr^{16} that $R_{1,16} = 3.60\ s^{-1}$ (which is very close to $R_{1,av} = 3.70\ s^{-1}$), and $R_{2,16} = 19.0\ s^{-1}$ (which differs considerably from $R_{2,av} = 14.7\ s^{-1}$). The intensities of the Thr^{16} cross peaks in the inverse detected 2D spectra are comparatively weak, which should also be the case in the 1D spectra. The C^β of Thr^{16} was calculated to give a positive contribution of less than 1% to the τ_R value determined from the 1D experiments. This means that the contribution to this τ_R from the local dynamics at the ends of the peptide is negative and circa 9%, which is partly compensated by the high R_2 of the β-carbon of Thr^{16}.

However, the accuracy of the present experiments does not support any more detailed conclusions. Nevertheless, it is important to note that an underestimate of 8% in τ_R is not large enough to affect the conclusions concerning solvation of P7 and absence of aggregation. In fact, any reasonable dimer configuration of P7 would, within the framework of the model of solvation discussed here, require a τ_R>4.4 ns, i.e., at least 17% larger than the value for the core region Leu^5-Arg^{19} determined from the 2D experiments. In the case of dimers, the solvation shell is entirely filled by water molecules, which is unrealistic for P7 which shows a high degree of helicity in the mixed solvent water/1,1,1,3,3,3-hexafluoro-2-propanol.

CONCLUSIONS

The peptide P7, PAADLARYRHYINLITRQRY-NH_2, dissolved in a mixture of water and 1,1,1,3,3,3-hexafluoro-2-propanol (70/30% v/v) at pH 3.1, is mainly α-helical in structure, as determined by CD spectroscopy and 2D ^{1}H NMR. The α-helical structure of residues Leu^5-Arg^{19} is well described by NMR-derived distance and angular restraints, while the structures of the residues of the N- and C-termini, i.e. Pro^1-Asp^4 and Tyr^{20}, are less well determined. The ^{13}C relaxation data of the individual C^α carbons, obtained by 2D NMR experiments with ^{13}C at natural abundance, show that the backbone of the α-helix, Leu^5-Arg^{19}, has uniform dynamics, well described by a singular rotational correlation time. The ^{13}C relaxation data of residues Pro^1-Asp^4 and Tyr^{20} show large effects from fast local dynamics. The 1D ^{13}C NMR experiments give average relaxation rates for all C^α carbons of the peptide. A single rotational correlation time may be derived which, for a largely helical peptide like P7, underestimates the real overall rotational correlation time by less than a few per cent. For P7 the rotational correlation time was determined at several temperatures over the range 10–45 °C. The effective molecular volume is found to be the same over the whole temperature range. From the value of the effective molecular volume it is concluded that the peptide is monomeric in solution, and is solvated by both water and cosolvent molecules. The application of 1D NMR-determined ^{13}C relaxation rates of C^α carbons, with ^{13}C at natural abundance or enriched, should be a useful and fast approach to determine the aggregation state of structured peptides and small proteins. Measurements at a single temperature may often be sufficient, but data at two or more temperatures will make certain whether an equilibrium between aggregation states occurs or not.

ACKNOWLEDGEMENTS

We would like to thank Ms. Britt-Marie Olsson for manually synthesising the peptide and Dr. Mats Andersson, Department of Medical Biochemistry and Biophysics, Laboratory Biochemistry 2, Karolinska Institute, Stockholm, and Ms. Olsson for the HPLC purification. Associate Professor Ülo Langel, Department of Neurochemistry and Neurotoxicology, Stockholm University, is greatly acknowledged for assistance in cleavage and the determination of the molecular weight of the peptide. We are grateful to Dr. Björn Nilsson at the Pharmacia Bioscience Center, Stockholm, for kindly giving us permission to use the CD spectropolarimeter. The authors also would like to thank The Swedish NMR Center, Stockholm, for letting us run the 500 MHz NMR spectrometer. Mr. Torbjörn Astlind is acknowledged for skilled computer assistance. A fellowship to J.J. from the Wenner-Gren Center Foundation is gratefully acknowledged. This work was

supported by grants from the Magnus Bergvall Foundation, the Carl Trygger Foundation for Scientific Research, the Erna and Victor Hasselblad Foundation, the Swedish Natural Science Research Council, and the Swedish National Board for Industrial and Technical Development (NUTEK).

REFERENCES

Abragam, A. (1962) *The Principles of Nuclear Magnetism*, 2nd ed., Clarendon Press, Oxford, pp. 294–297.
Arvidsson, K., Land, T., Langel, Ü., Bartfai, T. and Ehrenberg, A. (1993) *Biochemistry*, **32**, 7787–7798.
Arvidsson, K., Langel, Ü. and Ehrenberg, A. (1994) *Eur. J. Biochem.*, in press.
Barbato, G., Ikura, M., Kay, L.E., Pastor, R.W. and Bax, A. (1992) *Biochemistry*, **31**, 5269–5278.
Cantor, C.R. and Schimmel, P.R. (1980) *Biophysical Chemistry Part II: Techniques for the Study of Biological Structure and Function*, W.H. Freeman, San Francisco, CA, p. 555.
Cowley, D.J., Hoflack, J.M., Pelton, J.T. and Saudek, V. (1992) *Eur. J. Biochem.*, **205**, 1099–1106.
Dyson, H.J., Rance, M., Houghten, R.A., Lerner, R.A. and Wright, P.E. (1988) *J. Mol. Biol.*, **201**, 161–200.
Greenfield, N. and Fasman, G.D. (1969) *Biochemistry*, **8**, 4108–4116.
Güntert, P., Braun, W., Billeter, M. and Wüthrich, K. (1989) *J. Am. Chem. Soc.*, **111**, 3997–4004.
Güntert, P., Braun, W. and Wüthrich, K. (1991a) *J. Mol. Biol.*, **217**, 517–530.
Güntert, P., Qiu Qian, Y., Otting, G., Müller, M., Gehring, W. and Wüthrich, K. (1991b) *J. Mol. Biol.*, **217**, 531–540.
Kay, L.E., Jue, T.L., Bangerter, B. and Demou, P.C. (1987) *J. Magn. Reson.*, **73**, 558–564.
Krstenansky, J.L. and Buck, S.H. (1987) *Neuropeptides*, **10**, 77–85.
Lipari, G. and Szabo, A. (1982) *J. Am. Chem. Soc.*, **104**, 4546–4559.
Mierke, D.F., Dürr, H., Kessler, H. and Jung, G. (1992) *Eur. J. Biochem.*, **206**, 39–48.
Minakata, H., Taylor, J.W., Walker, M.W., Miller, R.J. and Kaiser, E.T. (1989) *J. Biol. Chem.*, **264**, 7907–7913.
Nirmala, N.R. and Wagner, G. (1989) *J. Magn. Reson.*, **82**, 659–661.
Otting, G. and Wüthrich, K. (1988) *J. Magn. Reson.*, **76**, 569–574.
Palmer III, A.G., Rance, M. and Wright, P.E. (1991) *J. Am. Chem. Soc.*, **113**, 4371–4380.
Peng, J.W., Thanabal, V. and Wagner, G. (1991) *J. Magn. Reson.*, **95**, 421–427.
Redfield, C., Boyd, J., Smith, L.J., Smith, R.A.G. and Dobson, C.M. (1992) *Biochemistry*, **31**, 10431–10437.
Richarz, R. and Wüthrich, K. (1978) *Biopolymers*, **17**, 2133–2141.
Saudek, V. and Pelton, J.T. (1990) *Biochemistry*, **29**, 4509–4515.
Shaka, A.J., Keeler, J., Frenkiel, T. and Freeman, R. (1983) *J. Magn. Reson.*, **52**, 335–338.
Sober, H.A. (Ed.) (1970) *Handbook of Biochemistry, Selected Data for Molecular Biology*, CRC Press, Cleveland, OH, p. B-75.
States, D.J., Haberkorn, R.A. and Ruben, D.J. (1982) *J. Magn. Reson.*, **48**, 286–292.
Weiner, S.J., Kollman, P.A., Case, D.A., Singh, U.C., Ghio, C., Alagona, G., Profeta Jr., S. and Weiner, P. (1984) *J. Am. Chem. Soc.*, **106**, 765–784.
Wüthrich, K. (1986) *NMR of Proteins and Nucleic Acids*, Wiley, New York, NY.
Zuiderweg, E.R.P., Hallenga, K. and Olejniczak, E.T. (1986) *J. Magn. Reson.*, **70**, 336–343.